

Stronger correlations than dense coding with elementary quantum resources

Amélie Piveteau,¹ Jef Pauwels,² Emil Håkansson,^{1,3} Sadiq Muhammad,^{1,4} Mohamed Bourennane,¹ and Armin Tavakoli^{5,6}

¹*Department of Physics, Stockholm University, S-10691 Stockholm, Sweden*

²*Laboratoire d'Information Quantique, CP 225, Université libre de Bruxelles (ULB), Av. F. D. Roosevelt 50, 1050 Bruxelles, Belgium*

³*Hitachi Energy Research, Forskagränd 7, 72219 Västerås, Sweden*

⁴*Department of Applied Physics, Royal Institute of Technology (KTH), Stockholm 106 91, Sweden.*

⁵*Institute for Quantum Optics and Quantum Information - IQOQI Vienna, Austrian Academy of Sciences, Boltzmanngasse 3, 1090 Vienna, Austria*

⁶*Institute for Atomic and Subatomic Physics, Vienna University of Technology, 1020 Vienna, Austria*

(Dated: May 20, 2022)

Dense coding is the seminal example of how entanglement can boost quantum communication. By sharing an Einstein-Podolsky-Rosen (EPR) pair, dense coding allows one to transmit two bits of classical information while sending only one qubit [1]. In this letter we show in both theory and experiment that qubit communication assisted by a shared EPR pair is strictly more powerful than two classical bits in more general communication tasks, and that this advantage persists even when the Bell basis measurement, which is essential for dense coding [2–8], is replaced by more elementary measurements such as partial Bell state analysers [9, 10] or even product measurements. Our results reveal that the power of entanglement in enhancing quantum communications qualitatively goes beyond boosting channel capacities and that it can be harvested in simpler and scalable experiments.

Entanglement and quantum communication are both paradigmatic resources for quantum information science and crucial for understanding the nonclassical nature of quantum theory. The former has been studied for decades in Bell-type experiments [11–14], where communication between the parties is not allowed. The latter has, in more recent years, been extensively studied in prepare-and-measure experiments, where shared entanglement is absent [15–17]. It is therefore natural to investigate the most general scenario, featuring both entanglement and quantum communication.

Dense coding is a striking illustration of the power of entanglement-assisted quantum communication [18, 19] (Fig. 1a). A sender and receiver share an EPR pair $|\phi^+\rangle = \frac{1}{\sqrt{2}}(|00\rangle + |11\rangle)$. Operating only on her local qubit, the sender can create a global basis of four orthogonal maximally entangled states; the so-called Bell basis. Consequently, when her qubit is relayed to the receiver, two bits of information can be retrieved. This sharply contrasts scenarios without entanglement, in which a qubit can never carry more than one bit of information [20].

However, the general predictions of quantum theory, in the ubiquitous sender-receiver scenario, are more diverse than those associated to the reliable transmission of a message [21, 22]. When both entanglement and quantum communication are available, little is known about the predictions of quantum theory. Here, we focus on the dense coding resources, namely a qubit message and a shared EPR state, and showcase quantum correlations that cannot be reproduced

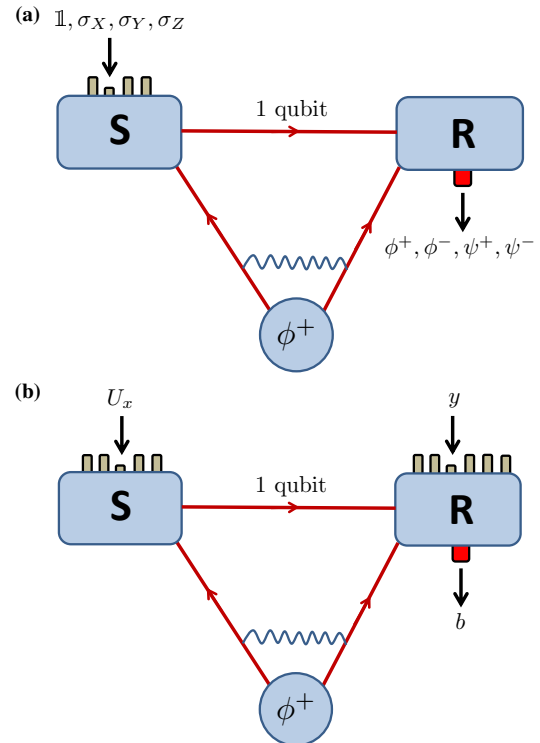


FIG. 1: (a) *Dense coding scenario.* The sender (S) and receiver (R) share an EPR pair $|\phi^+\rangle$. The sender selects one of four Pauli unitaries $\{\mathbb{I}, \sigma_X, \sigma_Y, \sigma_Z\}$, applies it to her qubit and relays it to the receiver who performs a measurement of both qubits in the basis of the four Bell states $|\phi^\pm\rangle = \frac{1}{\sqrt{2}}(|00\rangle \pm |11\rangle)$ and $|\psi^\pm\rangle = \frac{1}{\sqrt{2}}(|01\rangle \pm |10\rangle)$. From the outcome, the sender's two bit input can be recovered. (b) *Generic sender-receiver scenario.* The parties again share an EPR pair and are allowed to communicate a qubit. The sender can now select between any number of arbitrary unitary operations U_x and the receiver can select between any number of arbitrary quantum measurements.

by any dense coding protocol or, equivalently, any classical protocol using two bits of communication. Importantly, we show that the advantages can be detected using more elementary measurements than those required for dense coding. In fact, even product measurements can suffice. This enables simpler practical implementations, that circumvent the implementation of Bell basis measurements, and paves the way for entanglement-assisted quantum communication protocols that are scalable in both dimension and particle

number.

Consider a communication task in which the sender selects a classical input x and encodes it into a message that is sent to the receiver. The receiver selects a question, labeled y , to which he produces an answer labeled b . After many runs, they obtain probabilities $p(b|x, y)$. The parties pre-share the state $|\phi^+\rangle$ and the message consists of a single qubit, which is encoded via a local unitary U_x on the sender's share. Once the receiver holds both shares, he performs the measurement $\{E_{b|y}\}$. The probabilities are given by the Born rule,

$$p(b|x, y) = \text{tr} (E_{b|y} (U_x \otimes \mathbb{1}) \phi^+ (U_x^\dagger \otimes \mathbb{1})) . \quad (1)$$

Via dense coding, any $p(b|x, y)$, where x takes at most four values, can be generated in the experiment, regardless of the number of questions the receiver asks. Therefore, to find correlations that go beyond dense coding, one needs at least five values of x .

First, we show that there exists a natural information-theoretic task whose performance can be enhanced beyond what is possible with two bits. Consider a Random Access Code (RAC) [22]: the sender holds $x = x_1 x_2 \in \{1, 2, 3, 4\}^2$, and the receiver privately and uniformly selects $y \in \{1, 2\}$ with the aim of recovering x_y . This is a stochastic dense coding task, with average success rate $\mathcal{R} = \frac{1}{32} \sum_{x,y} p(b = x_y|x, y)$. Via dense coding, the receiver can, e.g., always recover x_1 but is then forced to guess the value of x_2 , yielding $\mathcal{R} = \frac{5}{8}$. In fact, no better two-bit strategy is possible (see methods). Nevertheless, this bound can be exceeded using the same quantum resources. Let the receiver measure the bases $|E_{b|1}\rangle = \mathbb{1} \otimes \sigma_X^{b_1} \sigma_Z^{b_2} |\phi^+\rangle$ and $|E_{b|2}\rangle = \mathbb{1} \otimes R |E_{b|1}\rangle$, where $R = \frac{1-i}{2\sqrt{2}} \mathbb{1} + \frac{1+i}{2\sqrt{2}} (\sigma_X + \sigma_Y + \sigma_Z)$ and $b = b_1 b_2 \in \{0, 1\}^2$. Given these measurements, the success rate is bounded by $\mathcal{R} \leq \frac{1}{32} \sum_x \max_{\{|\psi_x\rangle\}} \langle \psi_x | E_{x_1|1} + E_{x_2|2} | \psi_x \rangle = \frac{1}{32} \sum_x \lambda_{\max}(E_{x_1|1} + E_{x_2|2}) = \frac{3}{4}$, where λ_{\max} is the eigenvalue with the largest magnitude. This bound is reachable in our scenario because the eigenvector corresponding to λ_{\max} for each x (the optimal two-qubit state) is maximally entangled, and hence realisable via a local unitary on $|\phi^+\rangle$. As shown in methods, there exists no better quantum protocol.

However, the above advantage is based on performing a pair of (rotated) Bell basis measurements, i.e. measurements similar to that used in dense coding. With separate photons, such measurements lack both a simple implementation [23] and scalability (beyond two qubits). Moreover, even though essential for dense coding, it may not be that such sophisticated measurements are necessary for more general entanglement-assisted quantum communications. We therefore proceed to investigate whether advantages over dense coding can be preserved using considerably more elementary measurements.

To this end, consider a communication task with the minimal number of preparations needed to possibly beat two-bit protocols: the sender holds data $x \in \{1, \dots, 5\}$ and the receiver selects questions $y \in \{1, \dots, 6\}$, each with a binary answer $b \in \{+1, -1\}$ (see Fig. 1b). Clearly, in contrast to dense coding, each question can only yield partial knowledge about x . We consider a simple figure of merit, \mathcal{S} , in which

each question either has precisely one correct answer or no correct answer. We can rephrase this in terms of the answer $b = +1$ either being awarded one point (if correct), being penalised by one point (if incorrect) or being ignored. Our figure of merit is

$$\mathcal{S} \equiv \sum_{x=1}^5 \sum_{y=1}^6 c_{xy} p(b = +1|x, y) , \quad (2)$$

where the points awarded for each question are given by

$$c = \begin{pmatrix} 1 & 1 & 1 & 0 & 0 & 0 \\ -1 & 0 & 0 & 1 & 0 & 0 \\ -1 & 0 & 0 & -1 & 1 & 0 \\ 0 & -1 & 0 & -1 & -1 & 1 \\ 0 & 0 & -1 & -1 & -1 & -1 \end{pmatrix} . \quad (3)$$

This figure of merit comes with favourable properties, but may be viewed as a proof-of-principle construction.

Using two bits of communication, the optimal score is $\mathcal{S}_{2\text{ bits}} = 5$ (see methods). To saturate it, the two bits can be encoded as $\{x = 1, x = 2 \vee 3, x = 4, x = 5\}$. Indeed, dense coding substantially improves on the best standard classical protocol, based on one bit of communication, (at best $\mathcal{S}_{\text{bit}} = 3$) and even on the best protocol when one bit of communication is assisted by any amount of shared entanglement (at best $\mathcal{S}_{\text{ent+bit}} \approx 3.799$, see methods).

However we can beat the two-bit limit: this time using only simple entangled measurements that only discriminate one of the four Bell states. Let the sender perform the following unitaries on her share of $|\phi^+\rangle$,

$$U_1^S = \mathbb{1}, \quad U_2^S = \frac{-\sigma_Z \sqrt{3} - \sigma_X}{2}, \quad U_3^S = \frac{\sigma_X \sqrt{3} - \sigma_Z}{2}, \\ U_4^S = \frac{\mathbb{1} - i\sigma_Y \sqrt{3}}{2}, \quad U_5^S = \frac{\mathbb{1} + i\sigma_Y \sqrt{3}}{2} . \quad (4)$$

These are rotations in the XZ -plane of the Bloch sphere. Once the qubit is relayed, the receiver holds the state $U_x^S \otimes \mathbb{1} |\phi^+\rangle$. The receiver performs a binary-outcome measurement $\{|E_y\rangle\langle E_y|, \mathbb{1} - |E_y\rangle\langle E_y|\}$, where the outcome $b = +1$ corresponds to a projection onto the state $|E_y\rangle = U_y^R \otimes \mathbb{1} |\phi^+\rangle$ for some unitary U_y^R . Such a measurement may be viewed as a locally rotated partial Bell state analyser; it attempts to discriminate the maximally entangled state $|E_y\rangle$ from its orthogonal complement. We choose the unitaries of the receiver as

$$U_1^R = \mathbb{1}, \quad U_2^R = \frac{\nu_+ \mathbb{1} + i\nu_- \sigma_Y}{2\sqrt{2}}, \quad U_3^R = \frac{\nu_+ \mathbb{1} - i\nu_- \sigma_Y}{2\sqrt{2}}, \\ U_4^R = U_2^S, \quad U_5^R = U_3^S, \quad U_6^R = \frac{\mathbb{1} - i\sigma_Y}{\sqrt{2}} . \quad (5)$$

where $\nu_{\pm} = \sqrt{3} \pm 1$. Once again, these are rotations in the XZ -plane. The figure of merit becomes

$$\mathcal{S} = \sum_{x,y} c_{xy} |\langle E_y | U_x^S \otimes \mathbb{1} |\phi^+\rangle|^2 \\ = \frac{1}{2} \text{tr} \left[(U_y^R)^\dagger U_x^S \right] = 3 + \frac{3\sqrt{3}}{2} \approx 5.598 , \quad (6)$$

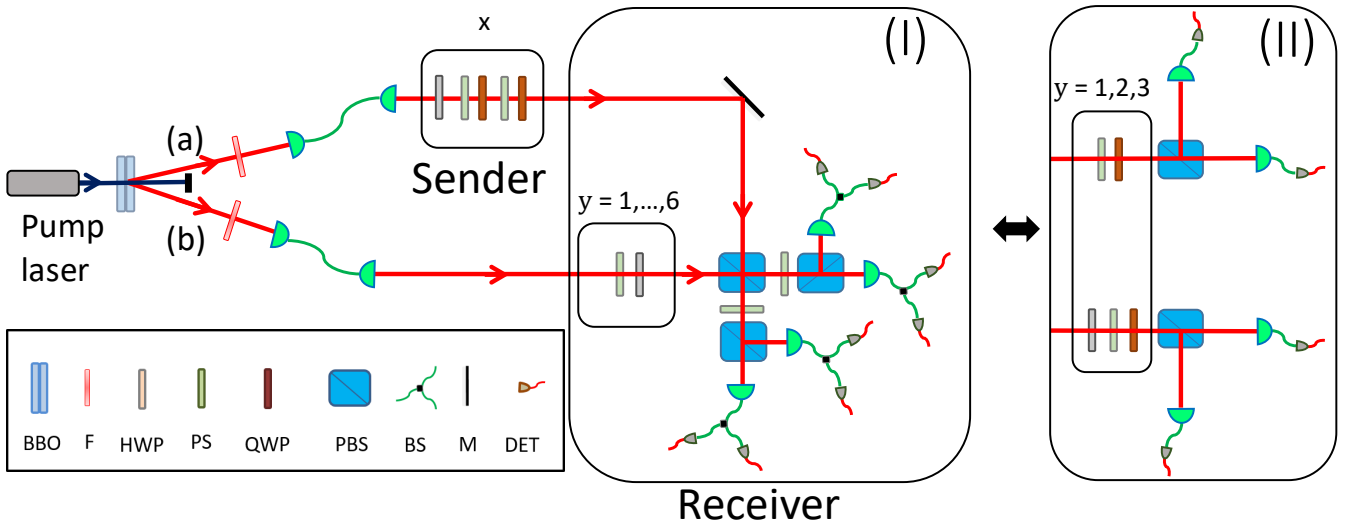


FIG. 2: Ultraviolet light centred at a wavelength of 390 nm is focused onto two 2 mm thick β barium borate (BBO) nonlinear crystals placed in cross-configuration to produce photon pairs emitted into two spatial modes (*a*) and (*b*) through the second order degenerate type-I SPDC process. The spatial, spectral and temporal distinguishability between the down-converted photons is carefully removed by coupling to single mode fiber, narrow Filter (F) and quartz wedges respectively and prepare $|\phi^+\rangle$. The unitaries of the sender and receiver are implemented using combination of half wave plates (HWP), quarter wave plates (QWP) and phase shifters (PS). (I) The partial Bell state measurements are implemented through two-photon interference, using PBS and HWP plates set at 22.5° . Beam splitters (BS) are introduced to estimate the projection probabilities before single photon detectors (actively quenched Si-avalanche photodiodes, DET). Outcome $b = +1$ corresponds to projection onto $|\phi^+\rangle$, and outcome $b = -1$ corresponds to the other Bell states $|\psi^-\rangle$, $|\psi^+\rangle$, and $|\phi^-\rangle$. In (II) partial Bell state measurement is replaced by product polarisation measurements and are performed by using HWPs, QWP and PBSs. Outcome $b \equiv b_1 b_2$, with $b_1, b_2 \in \{+1, -1\}^2$ corresponds to HH/VV or HV/VH detection when $b = +1$ or $b = -1$ respectively.

which considerably exceeds the two-bit limit¹. This protocol is also robust to unavoidable implementational imperfections. For instance, if the EPR pair is exposed to isotropic noise, so that the state becomes $v|\phi^+\rangle\langle\phi^+| + \frac{1-v}{4}\mathbb{1}$, for some visibility $v \in [0, 1]$, the advantage over dense coding is maintained whenever $v > \frac{16}{12+3\sqrt{3}} \approx 93\%$.

Thanks to the simplicity of the measurements, the correlation advantage can be demonstrated using standard linear optics for polarisation qubits. Using a spontaneous parametric down-conversion (SPDC) process, we prepare two-photon polarisation entangled state $|\Psi\rangle = \frac{1}{\sqrt{2}}(|HH\rangle + |VV\rangle)$. The single-qubit unitaries are implemented using combinations of wave-plates and phase shifters while the partial Bell state measurement is implemented by interfering the two photons via a polarising beam splitter. The setup is illustrated in Fig. 2 and the specific settings are given in Supplementary Material (SM). The average two-photon coincidences rate is about 2500 per second, which is ca. 13% of the singles rate. We benchmark the state preparation by measuring an average visibility of 0.992 ± 0.001 in the diagonal polarisation basis. Similarly, we benchmark the two-photon interference by a two-fold Hong-Ou-Mandel dip visibility of 0.961 ± 0.002 . For each setting x and y , we

collect on average 18 million events during a measurement time of two hours. The probabilities $p(b|x, y)$ are estimated from the relative frequencies (see SM). This leads us to the experimentally measured value of $\mathcal{S} = 5.379 \pm 0.009$, which outperforms the dense coding limit by approximately 40 standard deviations. Due to the sizeable violation and the large number of collected events, the p -value associated to our falsification of a two-bit model is vanishingly small. The result and its relation to the various theoretical limits is illustrated in Fig. 3.

However, even though partial Bell state measurements offer sizeable advantages over two-bit protocols in considerably simpler photonic experiments than dense coding, they do not offer a clear path to scalability in terms of dimension or particle number. Also, from a conceptual standpoint, it is not self-evident that entanglement in the measurement must, in general, be indispensable for correlation advantages. To address both the practical and conceptual question, we investigate the possibility of using even the most elementary class of joint measurements, namely product measurements, for entanglement-assisted communication beyond two-bit protocols.

Unfortunately, the previously discussed RAC seems to offer no such advantage. However, a variation of it, featuring a different number of inputs and settings, does reveal a distinct advantage. Let the sender hold data $x = x_1 x_2 x_3 \in \{0, 1\}^3$ and the receiver uniformly select $y \in \{1, 2, 3\}$ with the aim of recovering x_y . The average success rate is $\mathcal{T} = \frac{1}{24} \sum_{x,y} p(b = x_y|x, y)$. A two-bit protocol achieves at

¹ We note that the value (6) can be somewhat further increased. Using a numerical search, we find a protocol achieving $\mathcal{S} \approx 5.641$. However, this protocol is of lesser interest since it requires more complicated measurements.

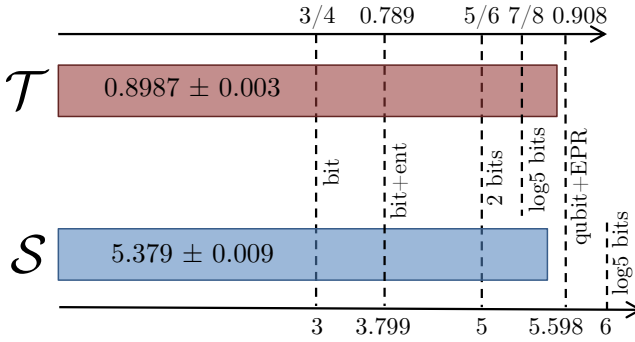


FIG. 3: Illustration of the experimentally measured performance of the communication tasks and their comparison to the best conceivable protocols based on one bit of classical communication, one bit of classical communication assisted by unbounded entanglement, two bits of classical communication and five-valued classical communication. The two-bit bound is equal to the maximum attainable value using a dense coding protocol. Another dashed line represents the theoretical value of the targeted quantum protocol, based on a shared EPR pair and a communicated qubit.

best $\mathcal{T}_{2\text{bit}} = \frac{5}{6}$. Now consider that the sender performs the unitaries

$$U_x = (-1)^{x_1} \begin{pmatrix} -\alpha_{x_1} \mu_{x_2 x_3} & (-1)^{x_2+x_3} \alpha_{\bar{x}_1} \mu_{x_2 x_3} \\ (-1)^{x_2+x_3} \sqrt{2} \alpha_{\bar{x}_1} & \sqrt{2} \alpha_{x_1} \end{pmatrix} \quad (7)$$

where $\mu_{x_2 x_3} = (-1)^{x_2} + i(-1)^{x_3}$, $\alpha_s = \frac{1}{2} \sqrt{1 + (-1)^s \sqrt{2/3}}$ and the bar-sign denotes bit-flip. The receiver measures three product observables $E_1 = \sigma_Z \otimes \sigma_Z$, $E_2 = \frac{1}{2} \sigma_Y \otimes (\sqrt{3} \sigma_Y + \sigma_Z)$ and $E_3 = \frac{1}{2} \sigma_X \otimes (\sqrt{3} \sigma_Y - \sigma_Z)$, where $E_y \equiv E_{1|y} - E_{2|y}$. This leads to $\mathcal{T} = \frac{1}{2} + \frac{1}{\sqrt{6}} > \mathcal{T}_{2\text{bit}}$. In fact, this outperforms even protocols based on sending five classical symbols. Interestingly, no better quantum protocol is possible, even if based on general entangled measurements (see methods). Adapting the optical setup (see Figure 2), we have demonstrated also this correlation advantage using the same source and the same measuring time as in the previous experiment. We observe $\mathcal{T} = 0.8987 \pm 0.003$, which beats the two-bit limit with over 20 standard deviations. The results are illustrated in Figure 3.

Our finding, that elementary measurements are sufficient for creating quantum correlations beyond the paradigmatic dense coding protocol, is based on departing from the study of reliable information transfer in favour of more general quantum communication tasks. Conceptually, it motivates a research effort into general entanglement-assisted correlations [24, 25] based on product measurements for the receiver. Understanding this resource for scalable tasks is also paired with noteworthy practical advantages since it circumvents the need for implementing highly demanding entangled measurements in favour of quantum devices that require only synchronised single-system measurements.

METHODS

Correlation bounds.— When communication is classical and no entanglement is present, $p(b|x, y)$ can be geometrically represented as a polytope whose vertices correspond to deterministic encoding and decoding schemes [15]. Consequently, the optimal performance of any linear figure of merit, e.g. that in Eq. (2), is necessarily attained at a vertex of this polytope. One can thus check the value of the figure of merit at all vertices and select the largest value. However, when (potentially unbounded) entanglement is added, this picture breaks down. Instead, upper bounds on \mathcal{S} and \mathcal{T} can be determined using the hierarchy of semidefinite programming relaxations developed in [24], which uses the concept of informationally-restricted quantum correlations [26, 27]. Using this method, and matching it with an explicit entanglement-based strategy with classical communication, we find $\mathcal{S}_{\text{ent+bit}} \approx 3.799$ and $\mathcal{T}_{\text{ent+bit}} \approx 0.789$.

The optimality of our protocols for the two RACs, corresponding to \mathcal{R} and \mathcal{T} , respectively, can be shown as follows. For both results, we use that the set of correlations attainable with an EPR pair and a qubit message is a subset of the set of correlations attainable in scenarios in which the sender and receiver only share classical randomness and communicate a four-dimensional quantum system. In these standard scenarios, it is known that $\mathcal{R} \leq \frac{3}{4}$ [28] and that $\mathcal{T} \leq \frac{1}{2} + \frac{1}{\sqrt{6}}$ [29] for general protocols. As our protocols saturate these bounds, optimality follows.

Statistical significance.— To express the statistical significance of our experimental results, we follow an approach similar to [30] introduced by [31], to which we refer for details. Consider the random variable

$$\hat{\mathcal{S}}_i = \sum_{xy} c_{xy} \frac{\chi(b_i = 1, x_i = x, y_i = y)}{p(x, y)}, \quad (8)$$

where i corresponds to the i th experimental run, $\chi(e)$ is the indicator function for the event e , i.e. $\chi(e) = 1$ if the event is observed and $\chi(e) = 0$ otherwise. For our experiment we simply chose $p(x, y) = 1/(6 \times 5) = 1/30$. The random variable $\hat{\mathcal{S}}_i$ may depend on past events, $j < i$, but not on future events, $j > i$. We define $\hat{\mathcal{S}} = \frac{1}{N} \sum_{i=1}^N \hat{\mathcal{S}}_i$ as our estimator for the value of our scoring function \mathcal{S} defined in (2), where $N \sim 18 \times 5 \times 6$ million is the total number of experimental rounds.

The Azuma-Hoeffding inequality implies that the probability p that dense coding or, equivalently, a two bit communication model will yield a value of \mathcal{S} greater or equal to the observed value is bounded by

$$p \left(\frac{1}{N} \sum_{i=1}^N \hat{\mathcal{S}}_i \geq \mathcal{S}_{\text{2bits}} + \mu \right) \leq \exp \left(\frac{2N\mu^2}{(c+T)^2} \right), \quad (9)$$

where $\mu = 0.379$ is the observed violation of the two bit bound, $T = 9$ is the classical 2-bit bound on $-\mathcal{S}$ and $c \equiv \max_{xy} c_{xy} / p(x, y)$. One finds that this probability is

vanishingly small. The analogous procedure applies to the data analysis based on the measured value of \mathcal{T} .

Experimental errors.— To reduce the multi-photons pairs emission we worked at a low rate (≈ 2500 pairs per sec) and increased the measurement time to reduce statistical errors. The impact of systematic errors was estimated using Monte Carlo simulation. These were reduced by using computerised high precision mounts. (See details in SM). The experiment is performed using the fair sampling assumption.

ACKNOWLEDGMENTS

We thank Stefano Pironio and Erik Woodhead for discussions and comments. This work was supported by the

Swedish research council, the Knut and Alice Wallenberg Foundation through the Wallenberg Center for Quantum Technology (WACQT), the Wenner-Gren Foundations and the Fonds National de la Recherche Scientifique F.R.S.-FNRS (Belgium) under a FRIA grant.

[1] C. H. Bennett and S. J. Wiesner, *Phys. Rev. Lett.* **69**, 2881 (1992).

[2] K. Mattele, H. Weinfurter, P. G. Kwiat, and A. Zeilinger, *Phys. Rev. Lett.* **76**, 4656 (1996).

[3] X. Li, Q. Pan, J. Jing, J. Zhang, C. Xie, and K. Peng, *Phys. Rev. Lett.* **88**, 047904 (2002).

[4] C. Schuck, G. Huber, C. Kurtsiefer, and H. Weinfurter, *Phys. Rev. Lett.* **96**, 190501 (2006).

[5] J. T. Barreiro, T.-C. Wei, and P. G. Kwiat, *Nature Physics* **4**, 282 (2008).

[6] L.-J. Kong, R. Liu, Z.-X. Wang, Y. Si, W.-R. Qi, S.-Y. Huang, C. Tu, Y. Li, W. Hu, F. Xu, Y.-Q. Lu, and H.-T. Wang, [arXiv:1709.03770 \[quant-ph\]](https://arxiv.org/abs/1709.03770) (2017).

[7] B. P. Williams, R. J. Sadlier, and T. S. Humble, *Phys. Rev. Lett.* **118**, 050501 (2017).

[8] J. Pauwels, S. Pironio, E. Z. Cruzeiro, and A. Tavakoli, [arXiv:2203.05372 \[quant-ph\]](https://arxiv.org/abs/2203.05372) (2022).

[9] H. Weinfurter, *Europhysics Letters* **25**, 559 (1994).

[10] S. L. Braunstein and A. Mann, *Phys. Rev. A* **51**, R1727 (1995).

[11] B. Hensen *et al.*, *Nature* **526**, 682 (2015).

[12] M. Giustina *et al.*, *Phys. Rev. Lett.* **115**, 250401 (2015).

[13] L. Shalm *et al.*, *Phys. Rev. Lett.* **115**, 250402 (2015).

[14] W. Rosenfeld, D. Burchardt, R. Garthoff, K. Redeker, N. Ortegel, M. Rau, and H. Weinfurter, *Phys. Rev. Lett.* **119**, 010402 (2017).

[15] R. Gallego, N. Brunner, C. Hadley, and A. Acín, *Phys. Rev. Lett.* **105**, 230501 (2010).

[16] J. Ahrens, P. Badziag, A. Cabello, and M. Bourennane, *Nature Physics* **8**, 592 (2012).

[17] M. Hendrych, R. Gallego, M. Mičuda, N. Brunner, A. Acín, and J. P. Torres, *Nature Physics* **8**, 588 (2012).

[18] C. H. Bennett, P. W. Shor, J. A. Smolin, and A. V. Thapliyal, *Phys. Rev. Lett.* **83**, 3081 (1999).

[19] C. H. Bennett, P. W. Shor, J. A. Smolin, and A. V. Thapliyal, *IEEE Transactions on Information Theory* **48**, 2637 (2002).

[20] A. S. Holevo, *Problems Inform. Transmission* **9**, 3 (1973).

[21] S. Wiesner, *SIGACT News* **15**, 78–88 (1983).

[22] A. Ambainis, A. Nayak, A. Ta-Shma, and U. Vazirani, in *Proceedings of the Thirty-First Annual ACM Symposium on Theory of Computing*, STOC '99 (Association for Computing Machinery, New York, NY, USA, 1999) p. 376–383.

[23] N. Lütkenhaus, J. Calsamiglia, and K.-A. Suominen, *Phys. Rev. A* **59**, 3295 (1999).

[24] A. Tavakoli, J. Pauwels, E. Woodhead, and S. Pironio, [arXiv:2103.10748 \[quant-ph\]](https://arxiv.org/abs/2103.10748) (2021).

[25] J. Pauwels, A. Tavakoli, E. Woodhead, and S. Pironio, [arXiv:2108.00442 \[quant-ph\]](https://arxiv.org/abs/2108.00442) (2021).

[26] A. Tavakoli, E. Zambrini Cruzeiro, J. Bohr Brask, N. Gisin, and N. Brunner, *Quantum* **4**, 332 (2020).

[27] A. Tavakoli, E. Z. Cruzeiro, E. Woodhead, and S. Pironio, [arXiv:2007.16145 \[quant-ph\]](https://arxiv.org/abs/2007.16145) (2020).

[28] A. Tavakoli, A. Hamed, B. Marques, and M. Bourennane, *Phys. Rev. Lett.* **114**, 170502 (2015).

[29] M. Navascués, A. Feix, M. Araújo, and T. Vértesi, *Phys. Rev. A* **92**, 042117 (2015).

[30] S. Pironio, A. Acín, S. Massar, A. B. de La Giroday, D. N. Matsukevich, P. Maunz, S. Olmschenk, D. Hayes, L. Luo, T. A. Manning, *et al.*, *Nature* **464**, 1021 (2010).

[31] R. D. Gill, *Foundations of Probability and Physics* **5**, 179 (2002).

[32] H. Anwer, S. Muhammad, W. Cherifi, N. Miklin, A. Tavakoli, and M. Bourennane, *Phys. Rev. Lett.* **125**, 080403 (2020).

[33] C. K. Hong, Z. Y. Ou, and L. Mandel, *Phys. Rev. Lett.* **59**, 2044 (1987).

SUPPLEMENTARY MATERIAL

Here we provide additional details on the experimental setup including details about the parties' unitary operations and how they are implemented, experimental error estimation and two-fold Hong-Ou-Mandel dip visibility.

A. Unitary operations in the experiment corresponding to figure of merit \mathcal{S}

Depending on her setting x , the sender applies the unitary transformations U_x^S , given by

$$\begin{aligned} U_1^S &= \mathbb{1}, & U_2^S &= \frac{-\sigma_Z \sqrt{3} - \sigma_X}{2}, & U_3^S &= \frac{\sigma_X \sqrt{3} - \sigma_Z}{2}, \\ U_4^S &= \frac{\mathbb{1} - i\sigma_Y \sqrt{3}}{2}, & U_5^S &= \frac{\mathbb{1} + i\sigma_Y \sqrt{3}}{2}. \end{aligned} \quad (10)$$

The receiver, in turn depending on his setting y , applies the unitary transformation U_y^R , given by

$$\begin{aligned} U_1^R &= \mathbb{1}, & U_2^R &= \frac{\nu_+ \mathbb{1} + i\nu_- \sigma_Y}{2\sqrt{2}}, & U_3^R &= \frac{\nu_+ \mathbb{1} - i\nu_- \sigma_Y}{2\sqrt{2}}, \\ U_4^R &= U_2^S, & U_5^R &= U_3^S, & U_6^R &= \frac{\mathbb{1} - i\sigma_Y}{\sqrt{2}}, \end{aligned} \quad (11)$$

where $\nu_{\pm} = \sqrt{3} \pm 1$. These unitary operations are realised in the experiment by rotating a half wave plate with rotation angle θ combined with a phase shift ϕ ,

$$U_z^K = \begin{pmatrix} \cos(2\theta_K^z) & \sin(2\theta_K^z) \\ e^{i\phi_K^z} \sin(2\theta_K^z) & -e^{i\phi_K^z} \cos(2\theta_K^z) \end{pmatrix}, \quad (12)$$

where $z = x$ for $K = S$ and $z = y$ for $K = R$.

The rotation angles θ_K^z and phases ϕ_K^z corresponding to each setting for the sender and receiver are listed in Table I and Table II respectively.

x	ϕ_S^x	θ_S^x
1	π	0
2	0	15
3	0	-30
4	π	-30
5	π	30

TABLE I: Half wave plate rotation angles θ_S^x and phase shifts ϕ_S^x applied by the sender for different settings x .

y	ϕ_R^y	θ_R^y
1	π	0
2	π	7.5
3	π	-7.5
4	0	15
5	0	-30
6	π	-22.5

TABLE II: Half wave plate rotation angles θ_R^y and phase shifts ϕ_R^y applied by the receiver for different settings y .

B. Experimental results for \mathcal{S}

Table III lists our experimental results alongside the theoretical probabilities for each combination of settings (x, y) associated to a non-zero payoff in the communication task ($c_{xy} \neq 0$). We also list the estimated errors, discussed below.

c_{xy}	$p(b x, y)$ Theory	$p(b x, y)$ Experiment	Errors
c_{11}	1	0.9725	0.0003
c_{21}	0	0.0250	0.002
c_{31}	0	0.0100	0.003
c_{12}	$(2 + \sqrt{3})/4$	0.9087	0.0006
c_{42}	$(2 - \sqrt{3})/4$	0.0610	0.001
c_{13}	$(2 + \sqrt{3})/4$	0.9198	0.0006
c_{53}	$(2 - \sqrt{3})/4$	0.0793	0.0009
c_{24}	1	0.9688	0.0003
c_{34}	0	0.0020	0.005
c_{44}	0	0.0050	0.004
c_{54}	0	0.0120	0.002
c_{35}	1	0.9828	0.0003
c_{45}	0	0.0240	0.002
c_{55}	0	0.0070	0.003
c_{46}	$(2 + \sqrt{3})/4$	0.9068	0.0006
c_{56}	$(2 - \sqrt{3})/4$	0.0560	0.001

TABLE III: Experimental results for \mathcal{S} .**C. Unitary operations in the experiment corresponding to figure of merit \mathcal{T}**

Depending on her setting x_1, x_2, x_3 , the sender applies the unitary transformations U_x , given by:

$$U_x = (-1)^{x_1} \begin{pmatrix} -\alpha_{x_1} \mu_{x_2 x_3} & (-1)^{x_2+x_3} \alpha_{\bar{x}_1} \mu_{x_2 x_3} \\ (-1)^{x_2+x_3} \sqrt{2} \alpha_{\bar{x}_1} & \sqrt{2} \alpha_{x_1} \end{pmatrix}, \quad (13)$$

where $\mu_{x_2 x_3} = (-1)^{x_2} + i(-1)^{x_3}$, $\alpha_s = \frac{1}{2} \sqrt{1 + (-1)^s \sqrt{2/3}}$ and the bar-sign denotes bit-flip. These unitary operations are realised in the experiment by two half wave plates and two quarter wave plates combined with a phase shift. The receiver makes the following measurements:

$$E_1 = \sigma_Z \otimes \sigma_Z, \quad E_2 = \frac{1}{2} \sigma_Y \otimes (\sqrt{3} \sigma_Y + \sigma_Z), \quad E_3 = \frac{1}{2} \sigma_X \otimes (\sqrt{3} \sigma_Y - \sigma_Z). \quad (14)$$

These measurements are realised in the experiment by a half wave plate and a quarter wave plate on the photon receiving the unitary and with a half wave plate with two quarter wave plates on the other photon. The rotation angles and phases corresponding to each setting for the sender and receiver are listed in Table IV and Table V respectively. Wave plates are named in the order of arrival for the photon, as shown in the figure in the main text.

$U_{x_1 x_2 x_3}$	phase	H_1	Q_1	H_2	Q_2
U_{000}	π	-8.816	45	33.75	45
U_{001}	0	-8.816	45	-78.75	45
U_{010}	0	-8.816	45	-33.75	45
U_{011}	π	-8.816	45	78.75	45
U_{100}	π	53.816	45	33.75	45
U_{101}	0	53.816	45	-78.75	45
U_{110}	0	53.816	45	-33.75	45
U_{111}	π	53.816	45	78.75	45

TABLE IV: Half and quarter wave plate rotation angles and phase shifts applied by the sender for different settings $U_{x_1 x_2 x_3}$.**D. Experimental results for \mathcal{T}**

Table VI lists our experimental results for each combination of unitary rotation $U_{x_1 x_2 x_3}$ and measurement E_y . We also list the estimated errors, as for the other experiment.

y	Mode1	Mode1	Mode2	Mode2	Mode2
	H_1	Q_1	Q_1	H_1	Q_2
1	0	0	0	0	0
2	0	-45	0	15	0
3	22.5	0	0	30	0

TABLE V: Half and quarter wave plate rotation angles applied by the receiver on each arms for different settings y .

$U_{x_1 x_2 x_3}$	Measurement	$p(b = x_y x, y)$ Theory	$p(b = x_y x, y)$ Experiment	error
U_{000}	E_1	0.9082	0.9139	0.01
U_{000}	E_2	0.9082	0.864	0.01
U_{000}	E_3	0.9082	0.9062	0.01
U_{001}	E_1	0.9082	0.9535	0.01
U_{001}	E_2	0.9082	0.8968	0.01
U_{001}	E_3	0.9082	0.8532	0.01
U_{010}	E_1	0.9082	0.9814	0.01
U_{010}	E_2	0.9082	0.8458	0.01
U_{010}	E_3	0.9082	0.8808	0.01
U_{011}	E_1	0.9082	0.9087	0.01
U_{011}	E_2	0.9082	0.8753	0.01
U_{011}	E_3	0.9082	0.9081	0.01
U_{100}	E_1	0.9082	0.8979	0.01
U_{100}	E_2	0.9082	0.9057	0.01
U_{100}	E_3	0.9082	0.9044	0.01
U_{101}	E_1	0.9082	0.8787	0.01
U_{101}	E_2	0.9082	0.8746	0.01
U_{101}	E_3	0.9082	0.9356	0.01
U_{110}	E_1	0.9082	0.8247	0.01
U_{110}	E_2	0.9082	0.9136	0.01
U_{110}	E_3	0.9082	0.9266	0.01
U_{111}	E_1	0.9082	0.9113	0.01
U_{111}	E_2	0.9082	0.905	0.01
U_{111}	E_3	0.9082	0.9044	0.01
$\mathcal{T} = \frac{1}{24} \sum_{x,y} p(b = x_y x, y)$		0.9082	0.8988	0.003

TABLE VI: Experimental results for \mathcal{T} .

E. Error estimation

Following [32] we consider error originating from the measurement side only. To reduce experimental errors in the measurements, we used computer controlled high precision motorised rotation stages to set the orientation of wave-plates with repeatability precision 0.02° for the first experiment and 0.025° for the second experiment. The use of different settings (x, y) induces a systematic error, which we estimate using Monte Carlo simulation. We assume that the wave-plates setting error is normally distributed with a standard deviation of 0.02° for the first experiment and 0.025° for the second experiment. This together with the Poissonian error in photon counting statistics comprise the final error reported here. Due to inefficiency in the single photon detectors, the photons are detected randomly and their counting is Poissonian. To decrease Poissonian counting error, we have chosen a measurement time of two hours for every setting and collected about 18 Million events. To guarantee that both parties receive single qubits, we worked at a low rate (≈ 2500 pairs per sec) to suppress higher order coincidence to almost 0.9 per sec.

F. Two-fold Hong-Ou-Mandel dip visibility

Bell state measurements are implemented through two-photon interference, using PBS and HWP plates set at 22.5° . The photons are detected by Si avalanche photodiodes and the coincidences are registered with an eight channels multifold coincidence counting unit. This Bell analyser consists of coherent interference at a polarisation beam splitter. To obtain indistinguishability of the photons, due to their arrival times, we adjusted the path length of one of the photons by using a

delay line [33]. In Figure 4, the coincidences between the detectors versus the delay path is shown. The zero delay corresponds to a maximal overlap (maximum indistinguishability). The interfering photons will bunch (they will exit only in one output arm of the PBS) causing the coincidence to vanish. The obtained visibility of the two-fold Hong-Ou-Mandel dip is 0.961 ± 0.002 .

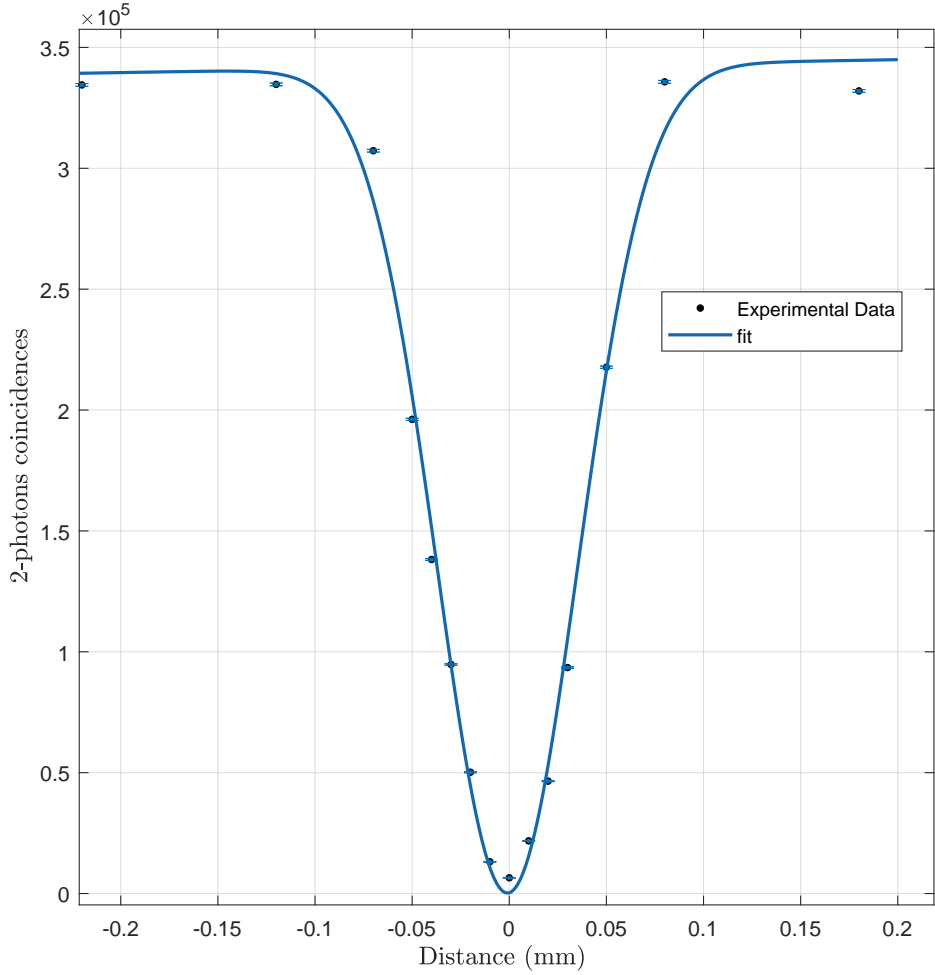


FIG. 4: Two-fold Hong-Ou-Mandel dip. The plot displays the two-fold photon counting coincidence versus the delay (the path difference between the two arms). The error bars indicate the Poissonian photon counting error statistics. The data is fitted with Gaussian function.

G. Random Access Code - \mathcal{R}

Consider a Random Access Code based on multi-valued inputs [28]. The sender has a total of 16 inputs, expressed as two pieces of data $x_1, x_2 \in \{1, 2, 3, 4\}$. The receiver randomly selects the data of interest, either choosing $y = 1$ for x_1 or $y = 2$ for x_2 . The aim is for the sender to encode (x_1, x_2) into a message such that the receiver can recover x_y with high average probability. The average success rate is given by $\mathcal{R} = \frac{1}{32} \sum_{x_1, x_2, y} p(b = x_y | x_1, x_2, y)$.

In the main text, we gave an explicit optimal strategy that achieves $\mathcal{R} = \frac{3}{4}$ in which the two measurements are mutually unbiased bases of maximally entangled states. It is interesting to note that in this quantum protocol, all winning probabilities are equal, i.e. $\forall (x_1, x_2, y)$ we have $p(b = x_y | x_1, x_2, y) = \frac{3}{4}$. Hence, the worst-case probability of recovering the data of interest is equal to the average probability \mathcal{R} .

If the EPR state is subject to isotropic noise, i.e. the effective state is $v|\phi^+\rangle\langle\phi^+| + \frac{1-v}{4}\mathbb{1}$, then the optimal strategy returns an advantage over protocols based on two bits of communication whenever $v > 3/4$. This is found immediately from solving $\frac{3}{4}v + (1-v)\frac{1}{4} = \frac{5}{8}$. The reason is that with probability v one plays the optimal strategy, achieving $\mathcal{R} = \frac{3}{4}$, while with probability $1-v$ one randomly guesses the output, achieving $\mathcal{R} = \frac{1}{4}$, which has to equate to the optimal success rate based on 2 bits, which is $\mathcal{R} = \frac{5}{8}$ [?].

The use of a maximally entangled qubit pair is essential in order to convey two bits with a single qubit message. To further elucidate the relationship between information capabilities and correlations created, we instead assign a pure partially entangled state $|\psi_\theta\rangle = \cos\frac{\theta}{2}|00\rangle + \sin\frac{\theta}{2}|11\rangle$, for $\theta \in [0, \frac{\pi}{2}]$. One expects the ability to convey information to grow with θ , from sending one bit when $\theta = 0$ to sending two bits when $\theta = \frac{\pi}{2}$. A natural way to quantify the information capability of such a partially entangled state is to consider the success rate with which the state can be used in dense coding. In other words, the largest probability of recovering a four-valued message x by applying a unitary transformation U_x to one share of the state and then extracting the information via a quantum measurement $\{M_b\}$. We therefore write

$$\mathcal{D}(\psi_\theta) = \max \frac{1}{4} \sum_{x=1}^4 p(b=x|x, \psi_\theta) = \max_{\{U_x\}, \{M_b\}} \frac{1}{4} \sum_{x=1}^4 \text{tr} \left[(U_x \otimes \mathbb{1}) |\psi_\theta\rangle \langle \psi_\theta| (U_x^\dagger \otimes \mathbb{1}) M_x \right]. \quad (15)$$

Following dense coding, we consider that the extraction measurement is a Bell basis measurement up to a local unitary, i.e. $M_b = |B_b\rangle \langle B_b|$ with $|B_b\rangle = V \otimes \mathbb{1} |\phi_b\rangle$, where the four states $|\phi_b\rangle$ are the Bell states $|\phi^+\rangle, |\phi^-\rangle, |\psi^+\rangle$ and $|\psi^-\rangle$. This simplifies the dense coding ability to

$$\mathcal{D}(\psi_\theta) = \max_{\{W_x\}} \frac{1}{4} \sum_{x=1}^4 |\langle \phi_x | (W_x \otimes \mathbb{1}) |\psi_\theta\rangle|^2, \quad (16)$$

where $W_x = V^\dagger U_x$. One can then see that the optimal unitaries are the same as in dense coding, namely $W_1 = \mathbb{1}$, $W_2 = \sigma_Z$, $W_3 = \sigma_X$ and $W_4 = \sigma_Y$. This gives $\mathcal{D}(\psi_\theta) = \frac{1+\sin\theta}{2}$. As expected, we see that the dense coding ability increases from 50% ($\theta = 0$) to 100% ($\theta = \frac{\pi}{2}$). We consider the critical degree of entanglement, i.e. the smallest value of θ , such that we can leverage a qubit message and a shared state $|\psi_\theta\rangle$ to beat the limit of a 2 bit strategy in the Random Access Code. We have numerically investigated this and the results are shown in Figure 5. As expected, we find that the success rate decreases as the dense coding capability decreases. Nevertheless, we are able to outperform the limit $\mathcal{R} = \frac{5}{8}$ whenever $\theta \gtrsim 0.6720$. This corresponds to $\mathcal{D} \approx 81\%$. Thus, quantum resources of a significantly smaller capacity still outperform two bits of communication in the Random Access Code.

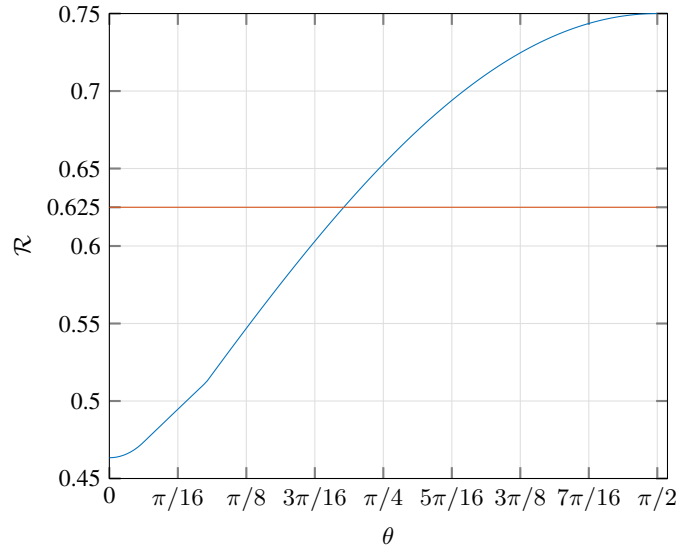


FIG. 5: Numerically obtained success rate in the Random Access Code versus the degree of entanglement in the shared state. The red horizontal line represents the best success rate based on 2 bits of communication. The success rate decreases as the entanglement weakens, because this reduces the dense coding capability of the channel. Above $\theta \gtrsim 0.6720$ the dense coding capability is still large enough to allow a quantum strategy to beat the success rate of 2 bit protocols.